

# A Simple Dynamical Model Capturing the Key Features of Central Pacific El Niño (Supporting Information Appendix)

Nan Chen and Andrew J. Majda

Department of Mathematics, and Center for Atmosphere Ocean Science, Courant Institute of  
Mathematical Sciences, New York University, 251 Mercer Street, New York, NY 10012 USA

This *SI Appendix* is formed by three sections. Section 1 contains a brief discussion of the derivations of the dynamical model and its low-order meridional truncation. The details of boundary conditions, numerical solvers as well as a list of the parameter values are also included. The mathematical formula of the Walker circulation is shown at the end of this section. Section 2 involves the basic information of the two-state Markov jump process that is utilized in the article. Section 3 contains more supporting information of the results. In Section 3.1, Hovmoller diagrams of atmospheric wind, ocean zonal current, thermocline depth and SST associated with the deterministic advective modes in different regimes are shown. In Section 3.2, the important roles of the stochasticity, the nonlinear advection and the mean easterly trade wind anomaly are all emphasized.

## 1 More details of the coupled model, meridional truncation and parameter choices

The coupled model considered in this article is derived from a more complicated model that consists of the skeleton model in the atmosphere [1, 2] coupled to a shallow water ocean in the long-wave approximation and a sea surface temperature (SST) budget with features from [3]. Then an asymptotic expansion with respect to a small factor  $\epsilon$  that is the ratio of intraseasonal time scale over the interannual one is applied and the result is Eq. (1)-(4) in the article. The details of model derivation are contained in the *SI Appendix* of [4]. For the convenience of statement, we summarize the coupled model below.

1. *Atmosphere model:*

$$\begin{aligned} -yv - \partial_x \theta &= 0, \\ yu - \partial_y \theta &= 0, \\ -(\partial_x u + \partial_y v) &= E_q / (1 - \bar{Q}). \end{aligned} \tag{A1}$$

2. *Ocean model:*

$$\begin{aligned} \partial_\tau U - c_1 YV + c_1 \partial_x H &= c_1 \tau_x, \\ YU + \partial_Y H &= 0, \\ \partial_\tau H + c_1 (\partial_x U + \partial_Y V) &= 0. \end{aligned} \tag{A2}$$

3. *SST model:*

$$\partial_\tau T + \mu \partial_x (UT) = -c_1 \zeta E_q + c_1 \eta H. \quad (\text{A3})$$

## 1.1 Meridional truncation

In order to compute the solutions of the coupled model, we consider the model in its simplest form, which is truncated meridionally to the first parabolic cylinder functions [5].

Different parabolic cylinder functions are utilized in the ocean and atmosphere due to the difference in their deformation radii. The first atmospheric parabolic cylinder function reads  $\phi_0(y) = (\pi)^{-1/4} \exp(-y^2/2)$ , and the third one that will be utilized as the reconstruction of solutions reads  $\phi_2 = (4\pi)^{-1/4} (2y^2 - 1) \exp(-y^2/2)$ . The oceanic parabolic cylinder functions read  $\psi_m(Y)$ , which are identical to the expressions of the atmospheric ones except depending on the  $Y$  axis.

In the atmosphere we assume a truncation of moisture, wave activity and external sources to the first parabolic cylinder function  $\phi_0$ . This is known to excite only the Kelvin and first Rossby atmospheric equatorial waves, of amplitude  $K_A$  and  $R_A$  [1, 2]. In the ocean, we assume a truncation of zonal wind stress forcing to  $\psi_0$ ,  $\tau_x = \tau_x \psi_0$ . This is known to excite only the Kelvin and first Rossby atmospheric oceanic waves, of amplitude  $K_O$  and  $R_O$ . Similarly, for the SST model we assume a truncation  $\psi_0$ ,  $T = T \psi_0$ . The ENSO model truncated meridionally reads:

1. *Atmosphere model:*

$$\begin{aligned} \partial_x K_A &= \chi_A (E_q - \langle E_q \rangle) (2 - 2\bar{Q})^{-1}, \\ -\partial_x R_A/3 &= \chi_A (E_q - \langle E_q \rangle) (3 - 3\bar{Q})^{-1}, \end{aligned} \quad (\text{A4})$$

2. *Ocean model:*

$$\begin{aligned} \partial_\tau K_O + c_1 \partial_x K_O &= \chi_O c_1 \tau_x / 2, \\ \partial_\tau R_O - (c_1/3) \partial_x R_O &= -\chi_O c_1 \tau_x / 3, \end{aligned} \quad (\text{A5})$$

3. *SST model:*

$$\partial_\tau T + \mu \partial_x ((K_O - R_O)T) = -c_1 \zeta E_q + c_1 \eta H, \quad (\text{A6})$$

where  $\chi_A$  and  $\chi_O$  are the projection coefficients from ocean to atmosphere and from atmosphere to ocean, respectively, due to the different extents in their meridional bases. The latent heating is linearized with  $E_q = \alpha_q T$  in the Pacific band and zero outside. Due to the absence of dissipation in the atmosphere, the solvability condition requires a zero equatorial zonal mean of latent heating forcing  $\langle E_q \rangle$  [6, 7]. Note that when meridional truncation is implemented, a projection coefficient  $\chi \approx 0.65$  appears in front of the nonlinear term [2], which here is absorbed into the nonlinear advection coefficient  $\mu$  for the notation simplicity and the parameter  $\mu$  in the Table below has already taken into account this projection coefficient.

Now instead of solving the coupled system (A1)–(A3), we solve the system (A4)–(A6). Periodic boundary conditions are adopted for the atmosphere model (A4). Reflection boundary conditions are adopted for the ocean model (A5),

$$K_O(0, t) = r_W R_O(0, t), \quad R_O(L_O, t) = r_E K_O(L_O, t), \quad (\text{A7})$$

where  $r_W = 0.5$  representing partial loss of energy in the west Pacific boundary across Indonesian and Philippine and  $r_E = 0.5$  representing partial loss of energy due to the north-south propagation of the coast Kelvin waves along the eastern Pacific boundary. Note that  $r_E$  here is different from the one taken in [4] ( $r_E = 1$ ), where a perfect reflection is assumed. For the SST model, no normal derivative at the boundary of  $T$  is adopted, i.e.  $dT/dx = 0$ .

To prevent nonphysical boundary layers in the finite difference method, the coupled model is solved through an upwind scheme, where some details of discretization is included in the *SI Appendix* of [4]. The total grid points in the ocean and in the atmosphere are  $N_O = 56$  and  $N_A = 128$ , respectively, which are doubled compared with that in [4] for the purpose of resolving some small scale interactions due to the nonlinearity. The time step is  $\Delta t = 4.25$  hours. The ratio  $\Delta t/\Delta x$  is approximately 0.115 under the nondimensional values.

The physical variables can be easily reconstructed in the following way.

$$\begin{aligned}
u &= (K_A - R_A)\phi_0 + (R_A/\sqrt{2})\phi_2, \\
\theta &= -(K_A + R_A)\phi_0 - (R_A/\sqrt{2})\phi_2, \\
v &= (4\partial_x R_A - \bar{H}A - S^\theta)(3\sqrt{2})^{-1}\phi_1, \\
U &= (K_O - R_O)\psi_0 + (R_O/\sqrt{2})\psi_2, \\
H &= (K_O + R_O)\psi_0 + (R_O/\sqrt{2})\psi_2.
\end{aligned} \tag{A8}$$

See [2, 4] for more details. The variables in (A8) are utilized in showing the Hovmoller diagrams in Figure 5 and 6 of the article.

## 1.2 Choices of parameters values

Two tables are included. Table 1 summarizes the variables in the coupled model and lists the associated units and the typical unit values. Table 2 shows the nondimensional values of the parameters that are utilized in the meridional truncated model.

## 1.3 Walker circulation

In the atmospheric model (skeleton model [1]), only the first baroclinic mode is included in the vertical direction, which has a profile of  $\cos(z)$  function. Also recall that the coupled model is projected to the leading parabolic cylinder function in the meridional direction, which has a Gaussian profile that centers at the equator. Thus, the meridional derivative at the equator is  $\partial_y\phi_0(y) = 0$  and the mass conservation equation reduces to

$$\tilde{u}_x(x, z) + \tilde{w}_z(x, z) = 0, \tag{A9}$$

where  $\tilde{u}(x, z)$  and  $\tilde{w}(x, z)$  are the zonal and vertical velocities, respectively, which are functions of both  $x$  and  $z$ . Recall that the zonal velocity can be written as [1]

$$\tilde{u}(x, z) = u(x) \cos(z). \tag{A10}$$

The vertical velocity that satisfy the mass conservation condition (A9) is given by

$$\tilde{w}(x, z) = w(x) \cos(z) = -u_x(x) \sin(z), \tag{A11}$$

Variable	unit	unit value
$x$ zonal axis	$[y]/\delta$	15000km
$y$ meridional axis atmosphere	$\sqrt{c_A/\beta}$	1500km
$Y$ meridional axis ocean	$\sqrt{c_O/\beta}$	330km
$t$ time axis intraseasonal	$1/\delta\sqrt{c_A\beta}$	3.3 days
$\tau$ time axis interannual	$[t]/\epsilon$	33 days
$u$ zonal wind speed anomalies	$\delta c_A$	5 $m s^{-1}$
$v$ meridional wind speed anomalies	$\delta[u]$	0.5 $m s^{-1}$
$\theta$ potential temperature anomalies	15 $\delta$	1.5K
$q$ low-level moisture anomalies	$[\theta]$	1.5K
$a$ envelope of synoptic convective activity	1	
$\bar{H}a$ convective heating/drying	$[\theta]/[t]$	0.45 $K \cdot day^{-1}$
$E_q$ latent heating anomalies	$[\theta]/[t]$	0.45 $K \cdot day^{-1}$
$T$ sea surface temperature anomalies	$[\theta]$	1.5K
$U$ zonal current speed anomalies	$c_O\delta_O$	0.25 $m s^{-1}$
$V$ zonal current speed anomalies	$\delta\sqrt{c}[U]$	0.56 $cm s^{-1}$
$H$ thermocline depth anomalies	$H_O\delta_O$	20.8 m
$\tau_x$ zonal wind stress anomalies	$\delta\sqrt{\beta/c_A}H_O\rho_Oc_O^2\delta_O$	0.00879 $N \cdot m^{-2}$
$\tau_y$ meridional wind stress anomalies	$[\tau_x]$	0.00879 $N \cdot m^{-2}$

Table 1: Definitions of model variables and units in the meridional truncated model.

Parameter	description	Nondimensional values
$c$	ratio of ocean and atmosphere phase speed	0.05
$\epsilon$	Froude number	0.1
$c_1$	ratio of $c/\epsilon$	0.5
$\chi_A$	Meridional projection coefficient from ocean to atmosphere	0.31
$\chi_O$	Meridional projection coefficient from atmosphere to ocean	1.38
$L_A$	Equatorial belt length	8/3
$L_O$	Equatorial Pacific length	1.16
$\gamma$	wind stress coefficient	6.529
$r_W$	Western boundary reflection coefficient in ocean	0.5
$r_E$	Eastern boundary reflection coefficient in ocean	0.5
$\zeta$	Latent heating exchange coefficient	8.5
$\alpha_q$	Latent heating factor	0.3782
$\bar{Q}$	mean vertical moisture gradient	0.9
$\mu$	nonlinear zonal advection coefficient	0.08
$a_p$	dissipation coefficient in the wind burst model	3.4

Table 2: Nondimensional values of the parameters.

where  $w(x) = -u_x(x)$ . In the dimensional form (variables with notation  $\cdot^D$ ),

$$w^D(x) = -\frac{[H_v]}{[L]}u_x^D(x), \quad (A12)$$

where  $[H_v] = 16/\pi\text{km}$  is the vertical length scale and  $[L] = 15000\text{km}$  is the horizontal length scale with nondimensional range  $x \in [0, 1.17]$ ,  $z \in [0, \pi]$ . The pair  $(\tilde{u}(x, z), \tilde{w}(x, z))$  forms the Walker circulation above the equatorial Pacific ocean as shown in Figure 7 of



the article.

## 2 Effective stochastic noise with a two-state Markov jump process

A two-state Markov jump process is adopted to generate effective stochastic noise that facilitates the intermittent occurrence of the central Pacific (CP) El Niño. The detailed set-up is included in [4] while more general background can be found in [8]. Here we summarize the necessary information that is utilized in the article.

Recall the evolution of wind burst amplitude  $a_p$ ,

$$\frac{da_p}{d\tau} = -d_p(a_p - \hat{a}_p(T_W)) + \sigma_p(T_W)\dot{W}(\tau), \quad (\text{A1})$$

where both  $\sigma_p$  and  $\hat{a}_p$  switch between one quiescent phase (State 0) and one active phase (State 1),

$$\begin{aligned} \text{State 0 } (s_0) : & \quad \sigma_p = 0.2, & \quad \text{and} & \quad \hat{a}_p = 0, \\ \text{State 1 } (s_1) : & \quad \sigma_p = 1.0, & \quad \text{and} & \quad \hat{a}_p = -0.25. \end{aligned}$$

The local transition probabilities between the two states for small  $\Delta t$  are given as follows,

$$\begin{aligned} P(X_{t+\Delta t} = s_1 | X_t = s_0) &= \mu_{01}\Delta t + o(\Delta t), \\ P(X_{t+\Delta t} = s_0 | X_t = s_1) &= \mu_{10}\Delta t + o(\Delta t), \\ P(X_{t+\Delta t} = s_0 | X_t = s_0) &= 1 - \mu_{01}\Delta t + o(\Delta t), \\ P(X_{t+\Delta t} = s_1 | X_t = s_1) &= 1 - \mu_{10}\Delta t + o(\Delta t), \end{aligned} \quad (\text{A2})$$

where  $X_t$  stands for either  $\sigma_p$  or  $a_p$  at time  $t$ . In (A2),  $\mu_{01}$  and  $\mu_{10}$  are the transition rates from State 0 to 1 and from State 1 to 0, respectively.

Due to the fact that an increase of the SST in the western Pacific leads to an enhanced wind burst activity, the active state corresponds to the instance when the western Pacific SST is high ( $T_W \geq 0$ ). On the other hand, since no strong wind burst is observed with a reduced SST in the western Pacific, a negative anomaly  $T_W \leq 0$  is linked with the quiescent state [9, 10, 11]. Given these facts, the following transition rates are utilized

$$\begin{aligned} \text{State 1 to 0: } \mu_{10} &= \frac{5}{6} \left( 1 - \tanh(2T_W) \right), \\ \text{State 0 to 1: } \mu_{01} &= \frac{1}{6} \left( \tanh(2T_W) + 1 \right). \end{aligned} \quad (\text{A3})$$

## 3 More supporting information of the results

### 3.1 Illustration of different fields associated with the deterministic nonlinear advective modes

Figure S1–S3 show the Hovmoller diagrams of atmosphere wind, ocean zonal current, thermocline height and anomalous SST at the equator that are associated with the deterministic nonlinear advective modes with mean easterly trade wind anomalies, where

$u_p = \hat{u}_p$ . These figures correspond to the three dynamical regimes shown in Panel (b)-(d) of Figure 3 in the article with the same parameters. As stated in the main article, corresponding to anomalous warm SST in the central Pacific, the ocean zonal current is westward and the rising branch of the Walker circulation shifts to the central Pacific region, which accompany with an eastern Pacific cooling with a shallow thermocline. Figure S4 shows a case with the intensification of a mean westerly trade wind anomaly. Reversed situation, including eastward zonal current and divergence of atmospheric surface wind in the central Pacific, is found.

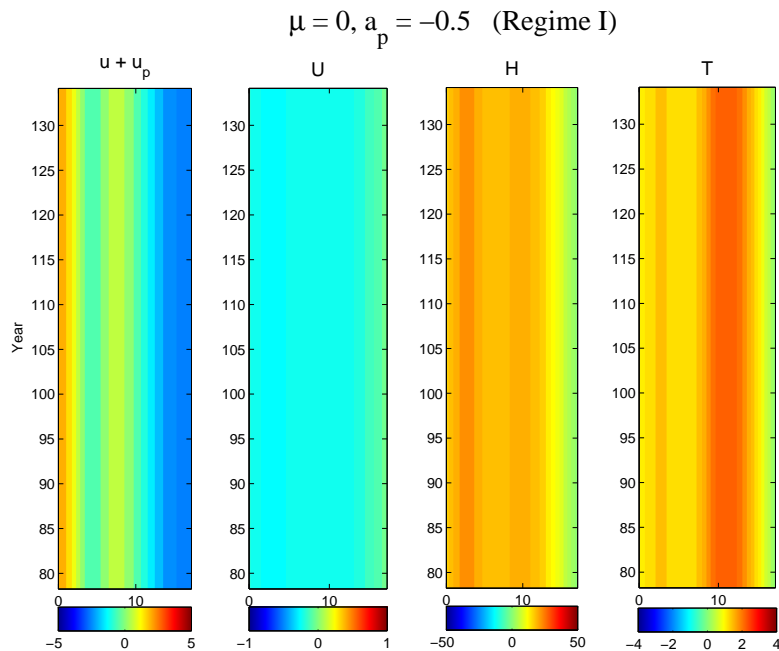


Figure S1: Hovmoller diagrams of atmospheric surface wind, ocean zonal current, thermocline depth and SST fields at the equator corresponding to Panel (b) of Figure 3 in the article (Regime I). Here  $u_p = \hat{u}_p = a_p s_p(x) \phi_0(0)$  has constant values along longitude lines.

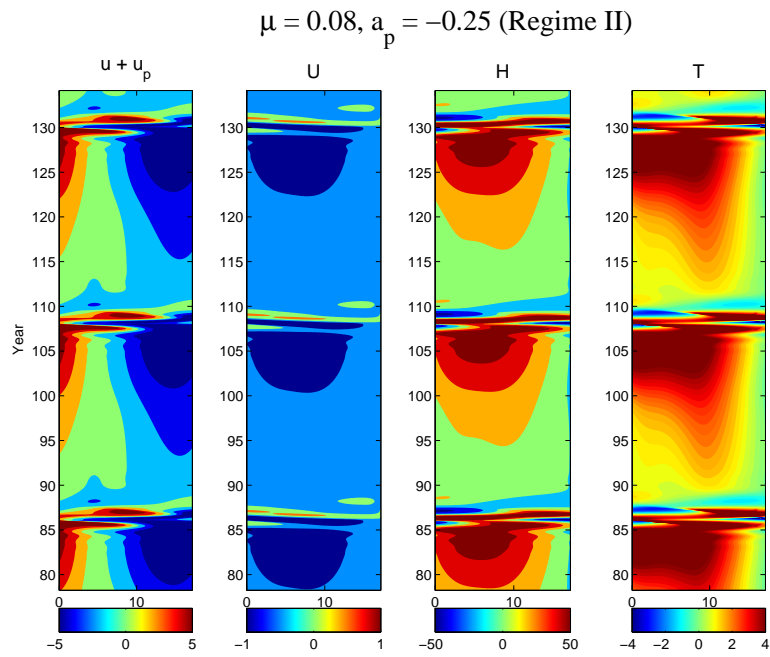


Figure S2: Hovmoller diagrams of atmospheric surface wind, ocean zonal current, thermocline depth and SST fields at the equator corresponding to Panel (c) of Figure 3 in the article (Regime II). Here  $u_p = \hat{u}_p = a_p s_p(x) \phi_0(0)$  has constant values along longitude lines.

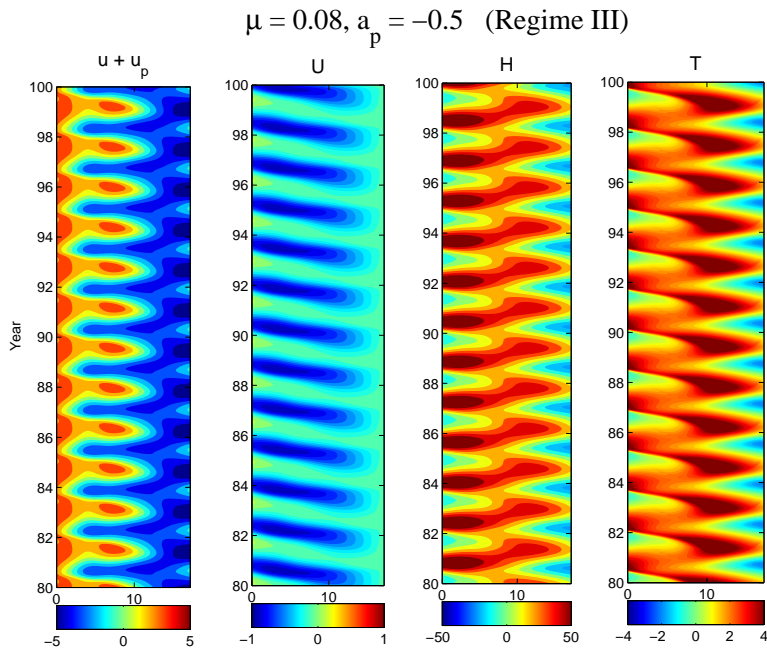


Figure S3: Hovmoller diagrams of atmospheric surface wind, ocean zonal current, thermocline depth and SST fields at the equator corresponding to Panel (d) of Figure 3 in the article (Regime III). Here  $u_p = \hat{u}_p = a_p s_p(x) \phi_0(0)$  has constant values along longitude lines. Note that the range of the y-axis is different from that in Figure S1 and S2.

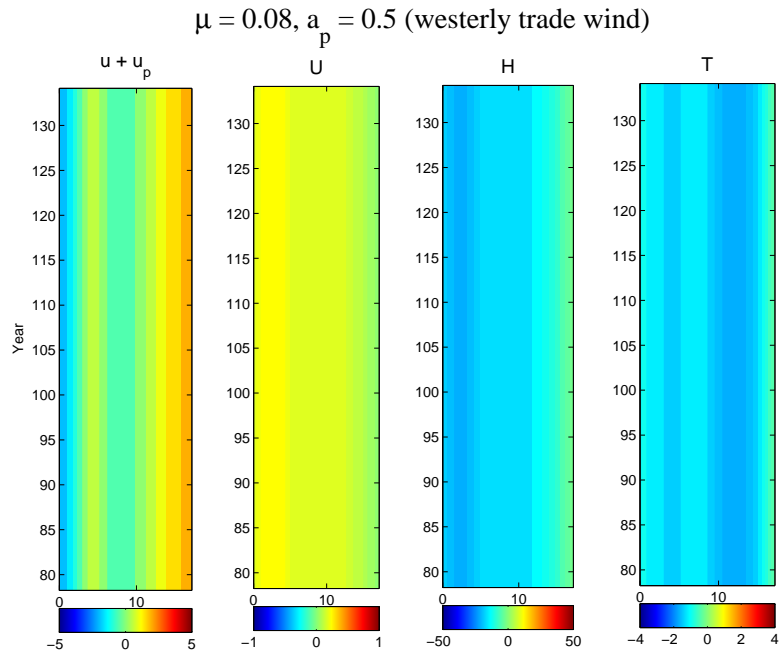


Figure S4: Hovmoller diagrams of atmospheric surface wind, ocean zonal current, thermocline depth and SST fields at the equator with a constant westerly trade wind anomaly. Here  $u_p = \hat{u}_p = a_p s_p(x) \phi_0(0)$  has constant values along longitude lines.

### 3.2 Roles of the nonlinear advection, mean easterly trade winds and stochasticity

Here, the roles of the nonlinear advection, mean easterly trade winds and stochasticity in wind model in generating the CP El Niño are further explored. These results are based on the coupled model, in which the stochastic wind burst process has an additive noise. In all the three cases below, except the difference in one or two parameters as will be pointed out, all the other set-up and the random number seeds are chosen to the same as those of Figure 4 in the article.

As shown in Figure 4 of the article, a moderate amplitude of the noise level  $\sigma_p \approx 1.0$  facilitates the occurrence of the CP El Niño events. Figure S5 includes the SST field with the same set-up but with an increase of  $\sigma_p$ . If the noise level  $\sigma_p$  is too large, then the effect from the stochasticity will dominate that from deterministic nonlinear advective modes. These stochastic winds represent strong westerly and easterly wind that trigger traditional El Niño and La Niña in the eastern Pacific ocean [4].

Figure S6 involves the situation that the coupled model has no zonal advection, i.e.,  $\mu = 0$ . With a mean easterly wind anomaly  $a_p$  and a moderate noise  $\sigma_p$ , anomalous warm SST occurs in the central-eastern Pacific, which is consistent with the deterministic convective mode shown in Figure S1. However, these warm SST anomalies cannot access the central and central-western Pacific regions as those shown in Figure 4–6 in the article. Clearly, the difference in the anomalous warm SST field is due to the difference in the budget from the flux divergence.

Figure S7 shows the results of the coupled model with a strong zonal advection but no easterly mean trade wind anomalies. Regardless of the noise level, very few central Pacific El Niño appears. In fact, in the absence of the mean easterly trade wind anomaly, moderate stochastic noise leads to very weak anomalous warm SST in the central-eastern Pacific. Due to such lack of the warm water source, almost no CP El Niño appears despite of the strong advection. On the other hand, strong stochastic noise only results in eastern Pacific El Niño, which is similar to those in Figure S5.

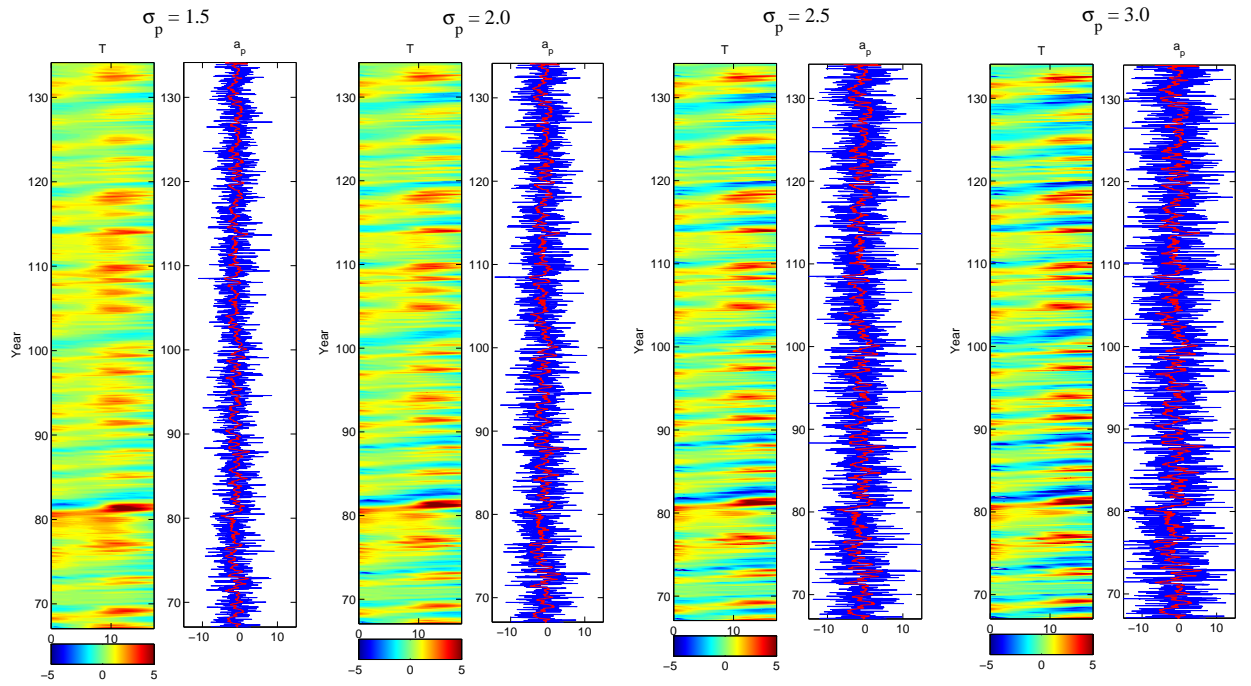


Figure S5: **Model with increased stochastic noise levels.** SST fields and the corresponding stochastic wind bursts with additive noise, where  $\sigma_p = 1.5, 2.0, 2.5$  and  $3.0$ , respectively. Both the other set-up and the seeds of random number generators are kept to be the same and as those of Figure 4 in the article.

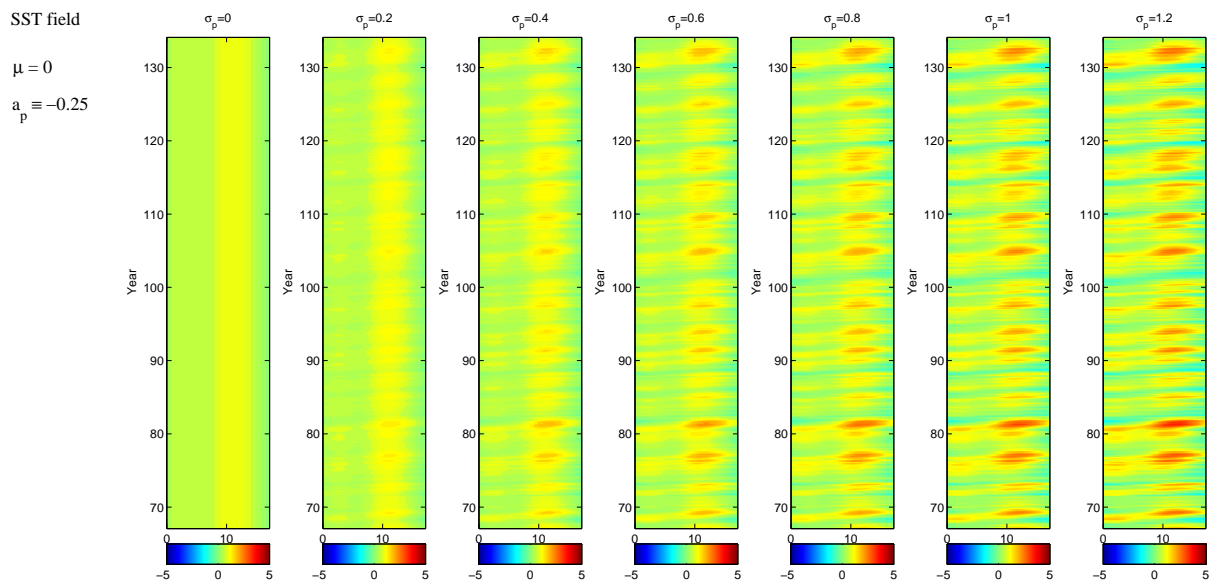


Figure S6: **Model without nonlinear zonal advection.** SST fields with different levels of additive stochastic noise in the wind burst model. Both the other set-up and the seeds of random number generators are kept to be the same and as those of Figure 4 in the article.



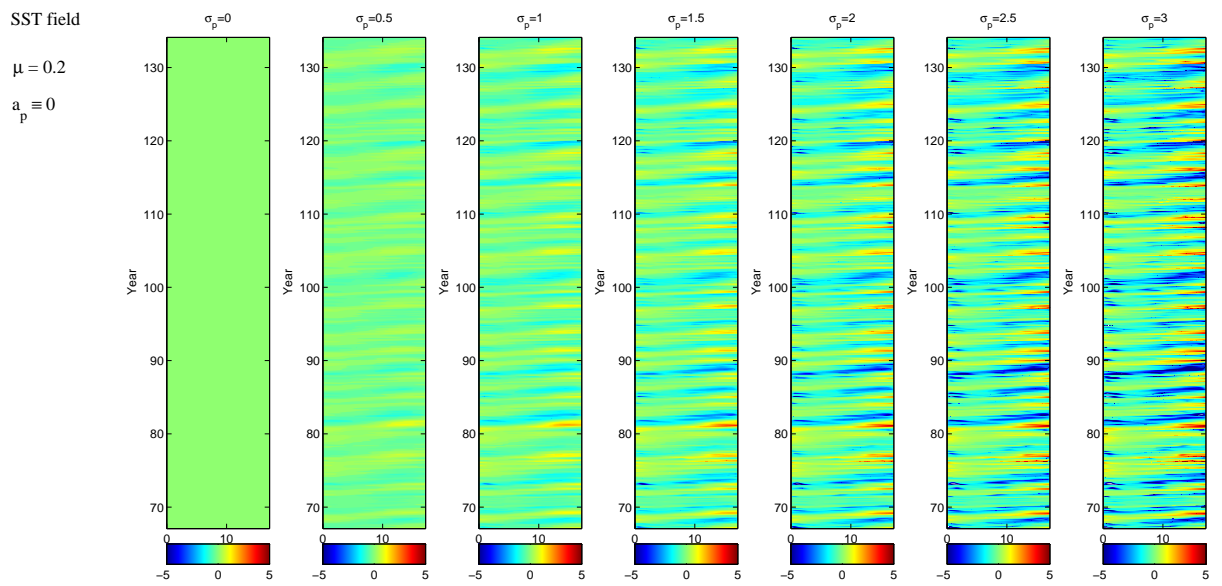


Figure S7: **Model without the intensification of the easterly trade wind.** SST fields with different levels of additive stochastic noise in the wind burst model. Both the other set-up and the seeds of random number generators are kept to be the same and as those of Figure 4 in the article.

## References

- [1] Majda AJ, Stechmann SN (2009). The skeleton of tropical intraseasonal oscillations. *Proceedings of the National Academy of Sciences*, 106(21):8417-22.
- [2] Majda AJ, Stechmann SN (2011). Nonlinear dynamics and regional variations in the MJO skeleton. *Journal of the Atmospheric Sciences*, 68(12):3053-71.
- [3] Moore AM, Kleeman R (1999). Stochastic forcing of ENSO by the intraseasonal oscillation. *Journal of Climate*, 12(5):1199-1220.
- [4] Thual S, Majda AJ, Chen N and Stechmann SN (2016). A simple stochastic model for El Niño with westly wind bursts. *Proceedings of the National Academy of Sciences*, Accepted.
- [5] Majda A (2003). Introduction to PDEs and Waves for the Atmosphere and Ocean. *American Mathematical Soc.*
- [6] Majda AJ, Klein R (2003). Systematic multiscale models for the tropics. *Journal of the Atmospheric Sciences*, 60(2):393-408.
- [7] Stechmann SN, Ogrosky HR (2014). The Walker circulation, diabatic heating, and outgoing longwave radiation. *Geophysical Research Letters*, 41(24):9097-105.
- [8] Majda AJ, Harlim J (2012). *Filtering complex turbulent systems*. (Cambridge University Press).
- [9] Tziperman E, Yu L (2007). Quantifying the dependence of westerly wind bursts on the large-scale tropical Pacific SST. *Journal of climate*, 20(12):2760-8.
- [10] Vecchi GA, Harrison DE (2000). Tropical Pacific Sea surface temperature anomalies, El Nino, and Equatorial Westerly Wind Events. *Journal of climate*, 13(11):1814-30.
- [11] Hendon HH, Wheeler MC, Zhang C (2007). Seasonal dependence of the MJO-ENSO relationship. *Journal of Climate*, 20(3):531-43.